

The Identification of a Dusty Grand Design Spiral Galaxy at $z = 3.06$ with JWST and ALMA

YUNJING WU,^{1,2} ZHENG CAI,³ FENGWU SUN,⁴ FUYAN BIAN,⁵ XIAOJING LIN,⁶ ZIHAO LI,⁶ MINGYU LI,⁶ FRANZ E. BAUER,^{7,8} EIICHI EGAMI,²
XIAOHUI FAN,² JORGE GONZÁLEZ-LÓPEZ,^{9,10} JIANAN LI,⁶ FEIGE WANG,^{2,*} JINYI YANG,^{2,†} SHIWU ZHANG,⁶ AND SIWEI ZOU⁶

¹Department of Astronomy, Tsinghua University, Beijing 100084, China ^c

²Steward Observatory, University of Arizona, 933 N Cherry Ave, Tucson, AZ 85721, USA

³Department of Astronomy, Tsinghua University, Beijing 100084, China ^d

⁴Steward Observatory, University of Arizona, 933 N Cherry Ave, Tucson, AZ 85721, USA ^e

⁵European Southern Observatory, Alonso de Córdova 3107, Casilla 19001, Vitacura, Santiago 19, Chile ^f

⁶Department of Astronomy, Tsinghua University, Beijing 100084, China

⁷Instituto de Astrofísica, Facultad de Física, Pontificia Universidad Católica de Chile Av. Vicuña Mackenna 4860, 782-0436 Macul, Santiago, Chile

⁸Millennium Institute of Astrophysics, Nuncio Monseñor Sótero Sanz 100, Providencia, Santiago, Chile

⁹Las Campanas Observatory, Carnegie Institution of Washington, Casilla 601, La Serena, Chile

¹⁰Núcleo de Astronomía de la Facultad de Ingeniería y Ciencias, Universidad Diego Portales, Av. Ejército Libertador 441, Santiago, Chile

ABSTRACT

Spiral arms serve crucial purposes in star formation and galaxy evolution. In this paper, we report the identification of “A2744-DSG-z3”, a dusty, grand-design-like spiral galaxy at $z = 3.059$ using the James Webb Space Telescope (JWST) NIRISS imaging and grism spectroscopy. A2744-DSG-z3 was discovered as a gravitationally lensed sub-millimeter galaxy with ALMA. This is the most distant grand-design stellar spiral structure seen thus far, consistent with cosmological simulations which suggest $z \approx 3$ as the epoch when grand-design spirals emerge. Thanks to the gravitational lensing and excellent spatial resolution of JWST, the spiral arms are resolved with a spatial resolution of ≈ 290 pc. Based on SED fitting, after correcting for lensing, the spiral galaxy has a de-lensed star formation rate of $85 \pm 30 M_{\odot} \text{ yr}^{-1}$, and a stellar mass of $\approx 10^{10.6} M_{\odot}$, indicating that A2744-DSG-z3 is a main-sequence galaxy. After fitting the spiral arms, we find a stellar effective radii ($R_{e,\text{star}}$) is 7.3 ± 0.8 kpc. Comparing to ALMA, we find that the effective radii ratio between dust and stars is ≈ 0.2 , similar to that of massive SFGs at $z \sim 2$, indicating a compact dusty core in A2744-DSG-z3. Moreover, this galaxy appears to be living in a group environment: including A2744-DSG-z3, at least three galaxies at $z = 3.05 - 3.06$ spectroscopically confirmed by JWST/NIRISS and ALMA, and residing within a lensing-corrected, projected scale of ≈ 70 kpc. This, along with the asymmetric brightness profile, further suggests that the spiral arms may be triggered by minor merger events at $z \gtrsim 3$.

Keywords: Spiral galaxies (1560) — Galaxy structure (622) — Galaxy formation (595) — Galaxy evolution (594) — Galaxy stellar disks (1594)

1. INTRODUCTION

Spiral structures are common among in local galaxies in the Universe. Some exhibit grand design morphologies, in which prominent and well-defined spiral arms can be deter-

mined, while other galaxies show multi-arm or flocculent spirals, with subtler structural features (Elmegreen et al. 2011; Elmegreen & Elmegreen 2014). Extensive efforts have been conducted to investigate the morphology, to understand the spiral/disk formation mechanism, and to study the relation between the spiral and star formation (e.g., Conselice 2014; Lin & Shu 1964). Nevertheless, when and how large spirals emerged in the early Universe is largely unknown.

Several studies have been conducted to search for spiral structures at $z \gtrsim 2$, the peak of cosmic star formation, and to study the initial formation and evolution of the spiral morphology (e.g., Margalef-Bentabol et al. 2022; Chen et al. 2022; Fudamoto et al. 2022). With ALMA, Tsukui & Iguchi (2021) discovered a cold, [C II]-emitting rotating

^c yj-wu19@mails.tsinghua.edu.cn

^d zcai@mail.tsinghua.edu.cn

^e fengwusun@arizona.edu

^f Fuyan.Bian@eso.org

* NHFP Hubble Fellow

† Strittmatter Fellow

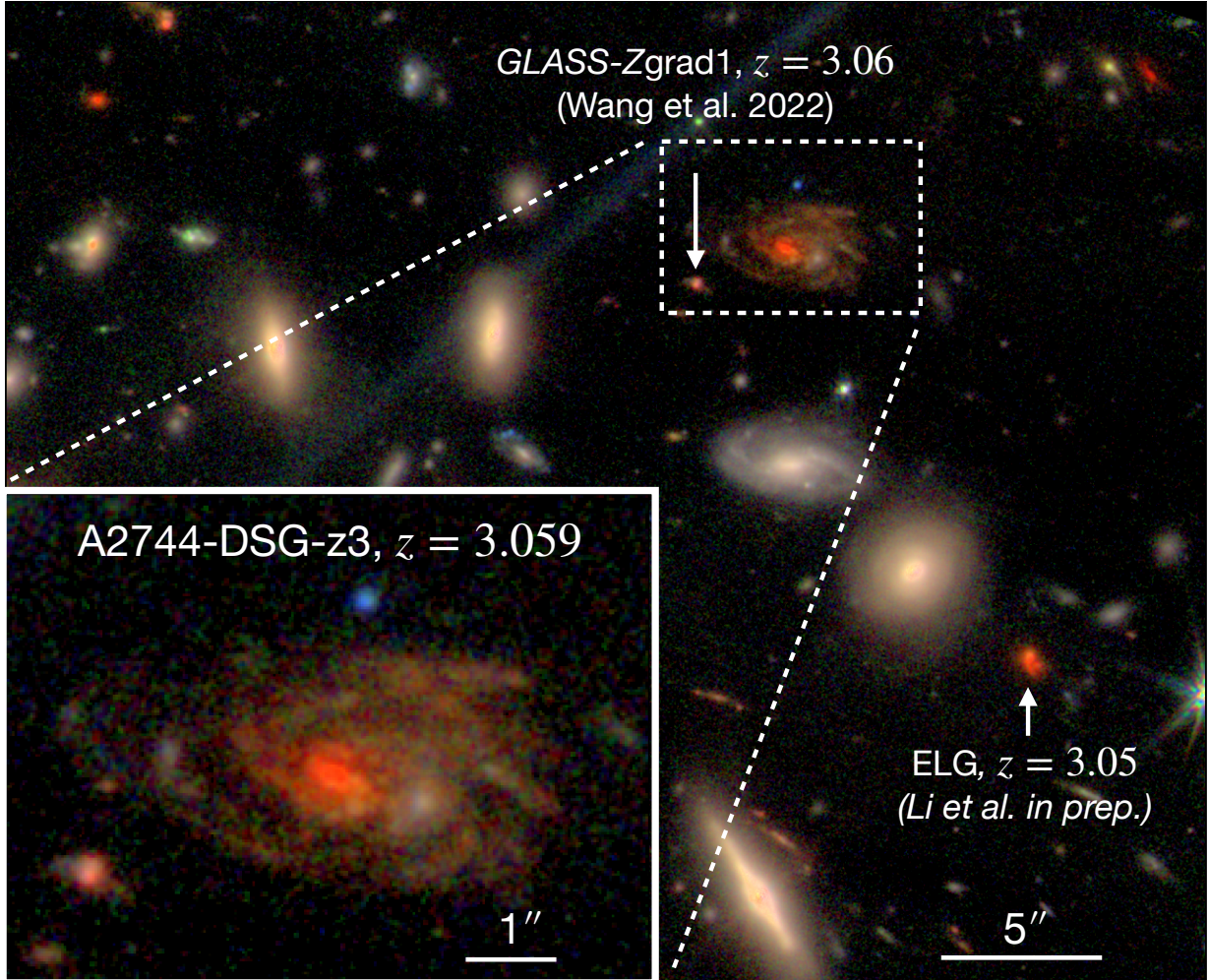


Figure 1. Dusty spiral galaxy (DSG) at $z = 3.059$. The composite RGB map of the target A2744-DSG-z3 is based on 3-band JWST/NIRISS imaging observations with pixel scale of $0.03''$ (blue: F115W, green: F150W, red: F200W). The target A2744-DSG-z3 was initially reported by the ALMA Frontier Fields survey (González-López et al. 2017; Laporte et al. 2017, A2744-ID03 in their papers) as a SMG (see also Sun et al. 2022). Meanwhile, the target GLASS-Zgrad1, reported in Wang et al. (2022), is a star-forming galaxy with stellar mass (M_*) of $\sim 10^9 M_\odot$ at same redshift. The impact parameter between these two galaxies is $\approx 3.1''$. One emission-line galaxy is confirmed by NIRISS grism and ALMA as well at $z = 3.05$ (Li et al. in prep.) with the projected separation of $15''$. This galaxy was also reported as a SMG with $M_{\text{dust}} \approx 10^{8.6} M_\odot$ (Laporte et al. 2017; Sun et al. 2022).

gaseous disk that can be interpreted as either spiral arms or tidal structures. Nevertheless, the stellar spiral structures are even rarer at high- z Universe. Only a small number of stellar spiral structures are identified at $z > 2$ that have been spectroscopically confirmed. HDFX 28 at $z = 2.011$ (Dawson et al. 2003), Q2343-BX442 at $z = 2.18$ (Law et al. 2012), and RS14, which is recently shown in JWST observations at $z = 2.46$ (Fudamoto et al. 2022). No grand-design-like stellar structures have yet to be confirmed at $z > 3$.

Currently, it is still unclear whether the rare appearance of spirals at high- z is mainly due to the spiral formation or due to surface brightness dimming. At $z > 2$, galaxies are observed to be clumpier and more irregular (e.g., Elmegreen et al. 2009). Law et al. (2009) suggest that the irregularity at $z \gtrsim 2$ can be explained, because the disks could be dy-

namically hot, and hot disks could yield more clumps than spiral structures (Conselice et al. 2005). Simulations further suggest that clumpy galaxies may transition into spirals. Nevertheless, at high- z , direct observational constraints linking gaseous clumps and spirals are lacking, while our understanding of how spirals may impact star formation remains unclear. For example, whether spirals at $z > 2$ can enhance the star formation or not are still under debated (e.g., Elmegreen 2002; Moore et al. 2012). All these questions or debates can be addressed by identification of more spirals across cosmic time and studying their star formation properties. Such observations can also answer the long-standing question of when and where grand-design-like spiral structures start to emerge in the early Universe, as well as what their evolutionary endpoints at present time might be.

In this paper, we present our identification of the very first grand-design stellar spiral at $z > 3$. This galaxy is reported as a submillimeter galaxy (SMG) with the ALMA Frontier Field survey (González-López et al. 2017; Laporte et al. 2017), and recovered recently with the ALMA Lensing Cluster Survey (ALCS; Sun et al. 2022) with updated spectroscopic redshift $z = 3.06$. Nevertheless, ALMA spatial resolution ($\approx 0''.6\text{--}1''.0$) is not sufficient to resolve most spiral-like structures for galaxies at $z \gtrsim 3$. JWST has a near-infrared (NIR) capability that can allow us to probe the stellar properties of high- z galaxies. The high spatial resolution ($\approx 0.06''$) enables the full resolving the spiral structures. In the following, we named it as A2744-DSG-z3 in the following of the paper, where DSG is the acronym of “dusty spiral galaxy”.

For SMGs, the rest-frame UV-optical morphological information (e.g., mergers, disks or spheroids) is largely unclear, due to their general faintness in these bands. Previous SMG-morphological analysis show disk-dominated features (Toft et al. 2014; Chen et al. 2022). However, as a SMG, A2744-DSG-z3 demonstrates spiral-arm-like features, suggesting that the formation mechanics of SMGs are not fully understood. Further, Davé et al. (2010) proposed that SMGs can form from isolated massive galaxies with starbursts, while, Sanders et al. (1988) suggest that merger processes are involved in forming SMGs. JWST studies of the rest-frame optical morphology to distinguish the above two formation scenarios.

This paper is organized as follows: Section 2, described details of data collection and reduction. Section 3, presents the spectra of A2744-DSG-z3 obtained from ALMA and JWST/NIRISS and a stellar-mass surface density map. In Section 4, provides further discussions of our observations. In this paper, we assume a flat cosmological model with $\Omega_M = 0.3$, $\Omega_\Lambda = 0.7$ and $H_0 = 70 \text{ km s}^{-1} \text{ Mpc}^{-1}$, $1'' = 7.7 \text{ kpc}$ at $z = 3.06$. The Glafic lensing model is adopted (Oguri 2010).

2. DATA

2.1. JWST/NIRISS imaging & grism observations

The NIRISS data were obtained from the GLASS JWST Early Release Science Program (Treu et al. 2022) with direct imaging in F115W, F150W, and F200W and grism spectroscopic observations. The direct-imaging exposure time is $2834.504 \text{ s} \approx 0.79 \text{ hours}$ per each band. The data were reduced using the standard JWST pipeline¹ v1.6.2 with calibration reference files “jwst_0944.pmap”. 1/f noise (see Schlawin et al. 2020) was modeled and removed using the

¹ <https://github.com/spacetelescope/jwst>

Table 1. Physical properties of A2744-DSG-z3.

Galaxy	A2744-DSG-z3
R.A. (deg)	3.58502
Dec (deg)	-30.38181
z_{spec}	3.059
μ	2.45
Physical parameters	
Inclination (deg)	28
Pitch angle (deg)	34 ± 13
Hubble type	Sc
SFR ($M_\odot \text{ yr}^{-1}$) ^a	85 ± 30
$\log[M_{\text{star}}/(M_\odot)]$	10.55
$\log[M_{\text{dust}}/(\mu^{-1}M_\odot)]$ ^a	8.70 ± 0.10
$R_{\text{e, star}}$ (kpc)	7.26 ± 0.75
$R_{\text{e, dust}}$ (kpc) ^b	2.04 ± 0.26

NOTE—^a. Reference of SFR and dust mass is from Sun et al. (2022), ^b. De-lensed result. Reference of effective radius of dust continuum: Sun et al. (in prep.).

code `tshirt`², and the “snowball” artifacts from cosmic rays (Rigby et al. 2022) were identified and masked. The world coordinate system of mosaicked images were registered using the Pan-STARRS1 catalog (Flewelling et al. 2020). The pixel scale of final mosaicked images is resampled to $0.03''$ with `pixfrac = 0.8`.

We reduced the grism data using the latest version of GRIZLI³. The contamination was subtracted by forward modeling of the full field-of-view (FoV) grism images. We secured reliable spectroscopic redshifts via spectral template fitting based on a library of spectral energy distributions (SED). The 2D grism spectra were drizzled using a pixel scale $0.065''$.

2.2. ALMA CO observations & the determination of redshift

Band 3 and 4 line-scan observations of our target are available in the ALMA archive (Program 2017.1.01219.S; PI: Bauer). The frequency ranges from 84.10–99.97 GHz and 139.51–155.38 GHz, covering emission lines CO (3-2) and (5-4) (rest-frame: 345.7960/576.2679 GHz) at $z = 3.06$ as reported in Sun et al. (2022). The on-source time of these observations is 12.5 and 10.0 mins. The spectra were directly extracted by rebinning the channel width to 74/69 km/s for CO(3-2) and CO(5-4) of available data products, using the CASA package v6.3.0 (McMullin et al. 2007).

3. ANALYSIS & RESULTS

In this letter, we focus on the physical properties of A2744-DSG-z3. Detailed information is listed in Table 1. Figure 1

² <https://github.com/eas342/tshirt>

³ <https://github.com/gbrammer/grizli/>

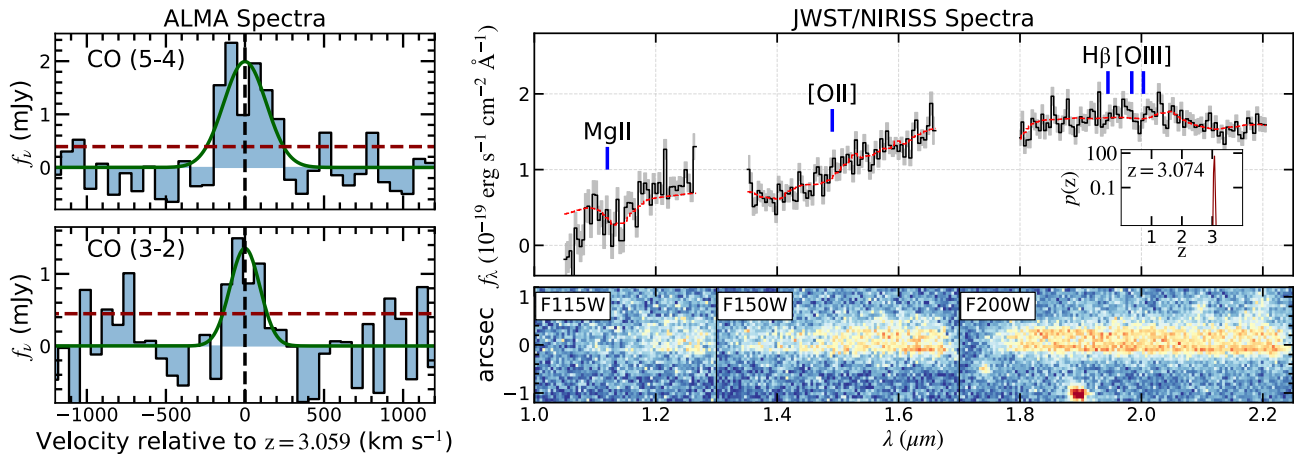


Figure 2. Determinations of the redshift of DSG-z3. **Left:** ALMA CO (5-4) and (3-2) spectra of A2744-DSG-z3. The dashed red line shows 1- σ noise spectra, while the dashed black line represents the systemic velocity. Dark-green curves show the best-fit Gaussian models of the spectra, indicating the CO-based redshift of $z_{\text{CO}} = 3.059 \pm 0.001$. **Right:** Top panel shows the optimally extracted 1D spectra from NIRISS 3-band grism observations. Black histogram denotes the observed flux density, with gray shadows showing 1 - σ errors. The dashed red lines are the GRIZLI modelled spectra containing continuum and nebular emission templates obtained by best SED fitting. The vertical blue lines mark the location of common emission lines ([O III], H β , [O II] and Mg II) which are not detected in DSG-z3. The subplot at bottom right shows the probability distribution function (PDF) of redshifts from SED-fitting, indicating the best grism redshift of this target is $z \approx 3.07$. Bottom panels are the joint two-dimensional spectra covered by NIRISS three filters (F115W, F150W and F200W).

shows the color composite map of this target. We note that there are two companion galaxies in the same field which could be related to A2744-DSG-z3. The first one is a star-forming dwarf galaxy close to A2744-DSG-z3, denoted as *GLASS-Zgrad1* (Wang et al. 2022). The initial offset is $\approx 3.1''$ on the image plane and then is delensed to $\approx 2''$. The second companion galaxy is on the southwest side of A2744-DSG-z3. The observed angular separation is $\approx 15''$, corresponding to a lensing-reconstructed impact parameter of $\approx 9.6''$ (i.e., ≈ 74 kpc at $z = 3$) (Li et al. in prep). The redshift of A2744-DSG-z3 is determined by ALMA CO observations (see the left panel of Figure 2). The redshifts of two companion galaxies are confirmed by the JWST/NIRISS [OIII]/H β spectroscopy. The right panel of Figure 2 shows the extracted 1D/2D grism spectra of A2744-DSG-z3. The grism spectra do not show obvious emission lines, while the 4,000 Å break is tentatively detected in F150W band. The best-fit redshift based on the grism spectra provided by GRIZLI is consistent with that determined by ALMA (see the probability density distribution in Figure 2).

3.1. Size Ratio between Dust and Stellar Components

Dust in the central few kpc region is likely generated by a central starburst, favoring an inside-out star-forming scenario (Nelson et al. 2016; Tadaki et al. 2020). Meanwhile, the rest-frame optical continua allows to probe the galaxy-scale star formation (Gullberg et al. 2019). Thus, the dust-to-stellar effective radius ratio ($R_{\text{e,dust}}/R_{\text{e,star}}$) reflects the comparison between two-component star-formation models (Lang et al. 2019; Tadaki et al. 2020; Sun et al. 2021). This dusty spiral galaxy, A2744-DSG-z3, provides us the opportunity to

connect the intense star-formation process and the structure formation of spiral arms and bulges.

To investigate the stellar component, we used reconstructed broad-band imaging observations that trace the rest-frame optical emission of A2744-DSG-z3. However, for star-forming galaxies, the size measured from the stellar density map would be more compact than that observed from surface brightness, which is due to the surface brightness dimming effects. (Wuyts et al. 2012; Genzel et al. 2020). Therefore, measuring half-light radius would overestimate the size of stellar mass. Fortunately, there is a strong empirical relation between stellar mass-to-light (M_{star}/L) ratio and the optical colors for spiral galaxies (e.g., Bell & de Jong 2001).

Following Lang et al. (2019), we derived the stellar mass based on broad-band color ($J_{115} - K_{200}$). Our photometric process is listed as follows. Firstly, we matched point-spread functions (PSFs). To construct PSFs in different filters, we selected stars from Gaia DR3 archival catalog (Gaia Collaboration et al. 2016, 2022) and then stacked unsaturated ones in the field-of-view. After matching PSFs to that of F200W, we performed pixel-pixel photometry in both J_{115} and K_{200} bands. The photometric zeropoints are determined using the calibration file “jwst_niriss_photom_0028.rmap”. The K-band observations and color maps are shown in the left two panels of Figure 3. In Figure 3, the spiral associated pixels were identified with the flux density over 2σ noise (determined by the pixel-to-pixel standard deviation).

We then obtained the stellar mass density (Σ_{Mstar}) map based on the relation between mass-to-light ratio and color. This relation was constructed and calibrated using simulated spectral energy distributions (SEDs) derived from stel-

lar population synthesis (SPS) methods (see appendix). The best-fit relation is:

$$M_{\text{star}}/L = 0.55 \times (J_{115} - K_{200}) + 18.92, \quad (1)$$

where the mass and luminosity are in solar units. We then obtained the pixelated $\Sigma_{M_{\text{star}}}$ map (third panel of Figure 3) with the M_{star}/L -color relation above. The radial profile of stellar surface density was measured by averaging that in de-projected galactocentric radii with a 1 kpc interval (see the last panel of Figure 3). The major axis of the galaxy was determined by the second-order moments of its stellar mass distribution relative to its mass density peak (Chen et al. 2021). The $R_{e,\text{star}}$ was calculated from the $\Sigma_{M_{\text{star}}}$ profile by defining as the radius containing half mass. The measured $R_{e,\text{star}}$ is 7.26 ± 0.75 kpc. We note that the $R_{e,\text{star}}$ was calculated by numerically integrating the mass density profile out to 20 kpc, approaching the outskirts of the disk.

The effective radius of the dust continuum at a rest-frame wavelength of $280 \mu\text{m}$ was measured using ALMA Band 6 data (2018.1.00035.L, PI: Kohno) through a UV-plane visibility profile modeling. The best-fit circularized effective radius assuming a Gaussian profile is $R_{e,\text{dust}} = 0.42 \pm 0.05''$, corresponding to a physical size of 2.04 ± 0.26 kpc after correcting for lensing magnification. This is consistent with the size derived assuming an exponential profile ($0.39 \pm 0.07''$), and the detailed methodology will be presented by Sun et al. (in prep.) among a larger sample of lensed dusty star-forming galaxies discovered with the ALCS (Sun et al. 2022). We conclude here that the measured radius ratio of A2744-DSG-z3 is $R_{e,\text{dust}}/R_{e,\text{star}} = 0.28 \pm 0.04$.

Furthermore, we measure the physical parameters of the observed spiral-arm like features. Following Law et al. (2012), we used the Logarithmic spiral equation (Davis et al. 2012):

$$r = r_0 e^{\theta \tan(\phi)}, \quad (2)$$

where r , r_0 , θ , and ϕ represent the radius, initial radius, angle, and pitch angle of arms, respectively. In the NIRISS-F200W imaging data, there are three spiral arms flowing into the red bulge, considering inclination effects, we fit the shape of them using Equation 2. The fitting results (blue lines in the left panel of Figure 3) show that the logarithmic equation effectively reproduces the arms. The fitted pitch angle of the arms is $\phi = 34 \pm 13^\circ$, similar to that of the grand-design spiral galaxy at $z = 2.18$ (Law et al. 2012).

4. DISCUSSION

4.1. Implication of the Observed Dust-to-stellar-radius Ratio

Different star-formation scenarios will predict different dust profiles (e.g., Nelson et al. 2016; Gullberg et al. 2019). To analyze the star-forming and structural properties, following Tadaki et al. (2020) and Sun et al. (2021), we compare the

main sequence offset (ΔMS) and the dust-to-stellar size ratio with those of dusty star-forming galaxies at $z \sim 2$. ΔMS is defined as the star-formation rate (SFR) ratio between the observed value and that expected on the so-called star-forming “main sequence” (SFR_{MS}), i.e., $\Delta\text{MS} = \log[\text{SFR}/\text{SFR}_{\text{MS}}]$ (Speagle et al. 2014). The observed SFR of A2744-DSG-z3 is $\log[\text{SFR}_{\text{obs}}/(\mu^{-1} M_\odot \text{ yr}^{-1})] = 2.32 \pm 0.16$ derived by SED-fitting results and reported in Sun et al. (2022). We follow Speagle et al. (2014) to calculate the SFR_{MS} ($\text{SFR}_{\text{MS}} = \text{SFR}_{\text{MS}}(M_{\text{star}}, z)$), using the stellar mass of A2744-DSG-z3 by summing up the de-lensed stellar-mass density map, which is $\log(M_{\text{star}}/M_\odot) = 10.55$. With an estimated main-sequence SFR of $\log[\text{SFR}_{\text{MS}}/(M_\odot \text{ yr}^{-1})]$ of ≈ 2.01 (de-lensed), the intrinsic ΔMS of A2744-DSG-z3 is ≈ -0.08 .

We compare our measurements with that of massive star-forming galaxies and SMGs at $z \sim 2$ (Lang et al. 2019; Tadaki et al. 2020) in Figure 4. For SMGs, the averaged $R_{e,\text{dust}}/R_{e,\text{star}}$ is close to 0.6 (blue shaded region). This means that the distribution of dust components is more compact than the stellar ones (e.g., Lang et al. 2019; Sun et al. 2021; Gómez-Guijarro et al. 2022), suggesting active bulge formation. This result is consistent with that observed from massive star-forming galaxies (blue dots in Figure 4; Tadaki et al. 2020). As a SMG, the observed radius ratio (0.28) of A2744-DSG-z3 is smaller than the previous studies, and those of local spirals ($R_{e,\text{dust}}/R_{e,\text{star}} \approx 1$; Hunt et al. 2015; Bolatto et al. 2017). Our results suggest that A2744-DSG-z3, as a spiral galaxy, is on the star-forming main sequence at $z \approx 3$ (similar to local spirals which are also on the MS), but hosts a more compact dust core than those of local spirals and high-redshift ($z \approx 2$) SMGs. For main-sequence spiral galaxies, the bulge size in the local universe is comparable with that of stellar components. This means that the bulges in the local universe are well evolved. However, for A2744-DSG-z3, at $z=3$, the bulge size is smaller than that of the stellar disk, suggesting a bulge formation scenario. A2744-DSG-z3 is undergoing intense star-formation in the central core region ($\lesssim 2$ kpc), surrounded by a more extended stellar disk (≈ 7 kpc).

4.2. Group Environment and the Formation of Spiral-like Structure at $z \gtrsim 3$

Thanks to the JWST/NIRISS grism observations, the target close to A2744-DSG-z3 (*GLASS* - Zgrad1, recently reported in Wang et al. 2022) is identified as one companion galaxy at the same redshift. The stellar mass of *GLASS* - Zgrad1 is $\approx 10^9 M_\odot$, and the de-lensed angular separation between the two sources is $\approx 2''$, corresponding to 15.4 kpc at $z = 3.06$. The stellar mass of A2744-DSG-z3 is $\approx 10^{10.6} M_\odot$, suggesting a halo mass of $\sim 10^{12.5} M_\odot$ (Rodríguez-Puebla et al. 2017; Somerville et al. 2018) with a Virial radius of ~ 120

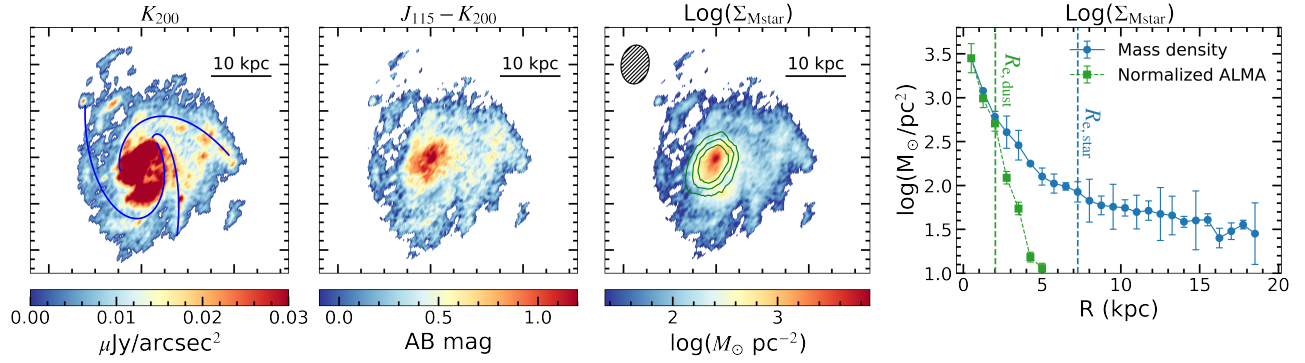


Figure 3. From left to right: Reconstructed K_{200} -band cutout map, $J_{115} - K_{200}$ color map, stellar surface density map, and lensing-corrected stellar-density/dust-continuum radial profile. Pixels belonging to A2744-DSG-z3 with fluxes higher than 2σ (determined by the pixel-pixel standard deviation) were shown. The stellar mass surface density map is derived based on a best-fit M_{star}/L vs. color relation. In the K_{200} -band map (Left panel), blue lines represent spiral arms fitted by the Logarithmic spirals equation (see Section 3.1, Eq. 2). Additionally, the ALMA dust-continuum observations are shown in the stellar surface density map (the third panel) as green contours ranging from $[5, 7.5, 10] \times \sigma$. In the right panel, we obtained the effective radius of stellar mass and dust continuum from the observed radial profile, i.e., $R_{e,\text{star}} = 7.26 \pm 0.75$ kpc, $R_{e,\text{dust}} = 2.04 \pm 0.26$ kpc.

kpc⁴. The lensing corrected projected separation between these two galaxies reside within the Virial radius. With the mass ratio between these two galaxies being ≈ 36 , this implies a minor-merger interaction scenario that potentially triggered the dusty central starburst in A2744-DSG-z3. Law et al. (2012) also suggest that one grand-design spiral galaxy at $z \sim 2$ could be formed by the minor merger process.

We note that, in the field A2744, Boyett et al. (2022) reported a number counts excess at $z \sim 3$. Thus, A2744-DSG-z3 could reside in an overdense region. For the companion galaxy, *GLASS* - Zgrad1, the measured slope in the metallicity distribution is $\Delta \log(\text{O}/\text{H})/\Delta r = 0.165 \pm 0.022$ (Wang et al. 2022). The occurrence of inverted gradients measured in this galaxy could also be explained by an ongoing minor merger. Due to the loss of angular momentum by the torque in the merger interactions, the metal-poor gas inflows into the inner disk to flatten/invert the metallicity gradient (Krabbe et al. 2011). Alternatively, the group environment may also give rise to enhanced cold mode accretion on the member galaxies, which inverts the metal gradient (Li et al. 2022).

To understand the environmental influence on the spiral formation, firstly, we note that the stellar spiral in A2744-DSG-z3 is present at $z = 3.06$, just around the peak of cosmic star formation (see Madau & Dickinson 2014 for a review). Thus, the number of galaxies and merger rates could be high. Cosmological simulations suggest that the high-redshift spiral structures may be due to higher merger rate (Hammer et al. 2009), high inflow rate, and the low angular momentum of cold streams (Cen 2014). Meanwhile, there are simulations reporting that the grand-design spirals exist by $z \approx 3$ (Fiacconi et al. 2015) and the high-redshift spirals

may be arisen from swing amplifications triggered by galaxy interactions. Kohandel et al. (2019) further showed that the cold gaseous spiral structure (close to the reionization epoch) can exist when the galactic disk is relaxed after a merger. A2744-DSG-z3 could experience merger and this could enhance the formation of spirals as predicted by cosmological simulations.

5. SUMMARY

In this Letter, we present the first identification of a dusty grand-design spiral galaxy (A2744-DSG-z3) at $z = 3.059$ observed by ALMA and JWST/NIRISS in both slitless-spectroscopic and direct imaging modes. The redshift of A2744-DSG-z3 is determined through ALMA CO observations. Meanwhile, by fitting the rest-frame optical continuum spectra provided by NIRISS/grism using GRIZLI, we also obtained a redshift solution of A2744-DSG-z3 with $z \approx 3.07$, consistent with that obtained from ALMA observations. The best-fit three spiral-arm models to the NIRISS/F200W direct images suggests an inclination/pitch angle of 28 (deg) and 34 ± 13 (deg), respectively. We convert the observed F115W-F200W colors and flux densities to stellar masses, and find a stellar-mass effective radius of 7.26 kpc, while the effective dust radius is 2.04 ± 0.26 kpc. Furthermore, the NIRISS grism data also identify a companion dwarf galaxy, called *GLASS* - Zgrad1 (Wang et al. 2022), with the projected separation of 15.4 kpc (de-lensed). The identification of this galaxy pair suggests a minor-merger scenario that triggers the dusty central starburst in A2744-DSG-z3.

The high spatial-resolution imaging observations provided by JWST give us the first opportunity to resolve the detailed structure of a spiral galaxy at $z \sim 3$ to a physical scale of ≈ 290 pc. Additionally, the NIRISS grism spectroscopic observations provides us the chance to determine redshifts for

⁴ <https://github.com/ylyu2010/DarkMatterHaloCalculator>

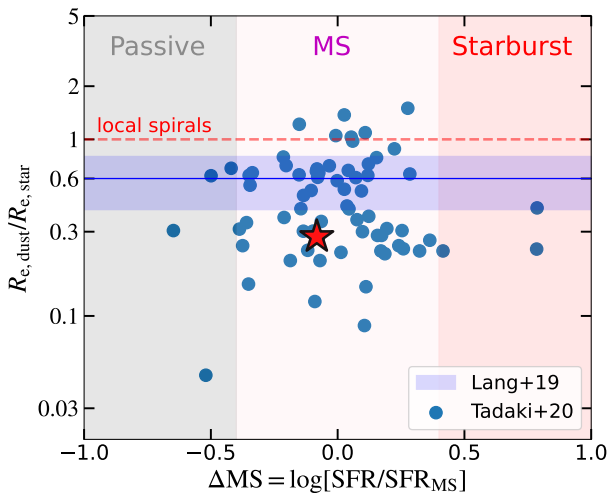


Figure 4. Dust and stellar effective radius ratio vs. main sequence offset (ΔMS). Blue dots are massive SFGs at $z \sim 2$ reported by Tadaki et al. (2020), while the red star represents the results of A2744-DSG-z3. Shaded blue region indicates the radius ratio observed of SMGs at $z \sim 2$ (Lang et al. 2019). ΔMS is defined as SFR ratios between the observed value and the expected ones on the star-forming MS. Following Aravena et al. (2020), the boundaries between passive, main sequence, and starburst galaxies are distinguished by $\Delta MS = \pm 0.4$, respectively. We conclude that, the spiral galaxy, A2744-DSG-z3, having a more compact dust core compared with SMGs at $z \sim 2$ and local spirals. And the star-forming intensity is the same as main-sequence galaxies at $z = 3$. Our observations suggest that for A2744-DSG-z3 at $z = 3$, the bulge was formed with intense star formation at the center core region ($\lesssim 2$ kpc).

bright targets or emitters within a sky coverage of $\sim 2'$. Like the galaxy pair identified in this work, spectroscopic redshifts through emission lines will further help us to investigate the environments of different galaxies at different redshifts.

The observed dust vs. stellar component radius ratio (0.28) of A2744-DSG-z3 suggests that the dust core is more compact than that observed of local spirals (≈ 1). The observed main sequence offset (-0.08) indicates that this target is undergoing the same intense star-formation activities as main-sequence galaxies at $z = 3$. Furthermore, the possibility of a minor-merger scenario may help to explain the observed inverted metallicity gradient of *GLASS* – Zgrad1 due to the interaction. We note that, future high spatial-resolution observations (e.g. ALMA CO for A2744-DSG-z3

and JWST/NIRSpec-IFU for *GLASS* – Zgrad1) will allow to probe the dynamics of this minor-merger candidate.

ACKNOWLEDGMENTS

Y.W. thanks Shude Mao, Zuyi Chen, and Xin Wang for very helpful discussions. Z.C., Y.W., X.L., Z.L., M.L., & S.Z. are supported by the National Key R&D Program of China (grant no. 2018YFA0404503) and the National Science Foundation of China (grant no. 12073014). F.S. acknowledges support from the NRAO Student Observing Support (SOS) award SOSPA7-022. F.S. and E.E. acknowledge funding from JWST/NIRCam contract to the University of Arizona, NAS5-02105. FEB acknowledges support from ANID-Chile BASAL CATA ACE210002 and FB210003, FONDECYT Regular 1200495 and 1190818, and Millennium Science Initiative Program – ICN12.009. F.W. is thankful for support provided by NASA through the NASA Hubble Fellowship grant no. HST-HF2-51448.001-A awarded by the Space Telescope Science Institute, which is operated by the Association of Universities for Research in Astronomy, Inc., under NASA contract NAS5-26555.

This work is based on observations made with the NASA/ESA/CSA James Webb Space Telescope. The data were obtained from the Mikulski Archive for Space Telescopes at the Space Telescope Science Institute, which is operated by the Association of Universities for Research in Astronomy, Inc., under NASA contract NAS 5-03127 for JWST. These observations are associated with program ERS-1324. The authors acknowledge the *GLASS* team for developing their observing program with a zero-exclusive-access period.

This paper makes use of the following ALMA data: ADS/JAO.ALMA#2017.1.01219.S. ALMA is a partnership of ESO (representing its member states), NSF (USA) and NINS (Japan), together with NRC (Canada), MOST and ASIAA (Taiwan), and KASI (Republic of Korea), in cooperation with the Republic of Chile. The Joint ALMA Observatory is operated by ESO, AUI/NRAO and NAOJ. In addition, publications from NA authors must include the standard NRAO acknowledgement: The National Radio Astronomy Observatory is a facility of the National Science Foundation operated under cooperative agreement by Associated Universities, Inc.

Facilities: JWST, ALMA

Software: astropy (Astropy Collaboration et al. 2013, 2018), BAGPIPES (Carnall et al. 2018), glafic (Oguri 2010)

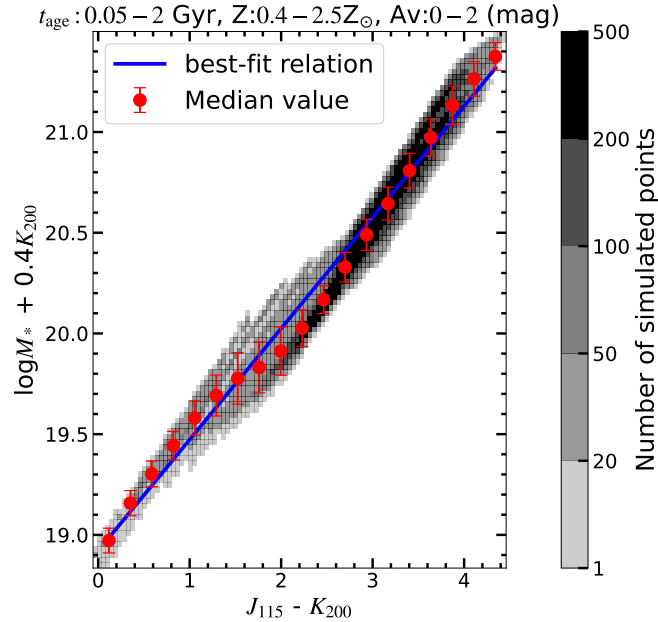


Figure 5. Simulated M_{star}/L vs. color relation. Gray-scale images represents the number of simulated data points with different stellar parameters (e.g., t_{age} , Z , and A_V). Stellar ages range from 50 Myr to 2 Gyr at $z = 3.06$, while metallicity ranges from 0.4 to 2.5 Z_{\odot} . The simulated colors are derived by adopting the Calzetti et al. (2000) law with $A_V = 0.0 - 2.0$ (mag). Red points are median values in different color bins, while error bars are standard deviations in each bin. The blue line is a best-fit linear relation using the median points.

APPENDIX A: MASS-TO-LIGHT RATIO VS. COLOR RELATION

Empirically, Bell & de Jong (2001) presented a strong correlation between stellar mass-to-light (M_{star}/L) ratio and the optical colors for spiral galaxies. Therefore, the JWST rest-frame optical and high spatial resolution observations give us the first opportunity to resolve the stellar mass distribution of a spiral galaxy at $z = 3.06$. To measure the pixelated stellar mass of A2744-DSG-z3, we follow the procedures in Lang et al. (2019). The M_{star}/L vs. color relation is constructed and calibrated by synthetic galaxy SEDs.

To generate mocked SEDs, we use a public python package BAGPIPES (Carnall et al. 2018) by adopting different stellar parameters (e.g., the age/metallicity of stellar populations t_{age}/Z , and the dust attenuation parameter in the rest-frame V band, A_V). For galaxy models, we assume a Kroupa (2002) initial mass function with t_{age} ranging from 0.05 – 2 Gyr, while Z ranges from 0.4 – 2.5 Z_{\odot} . Then, we assume an exponentially declining star formation history (SFR) with timescales of $\tau_{\text{SFR}} = 30$ Myr, which is guided by the best fitting result of a similar red spiral galaxy at $z \sim 2.5$ (Fudamoto et al. 2022). In order to convert these mocked galaxy SEDs to colors, we apply a Calzetti et al. (2000) dust-attenuation law with $A_V = 0.0 - 2.0$. Fig. 5 shows the M_{star}/L vs. color relation. We define the M_{star}/L as $(\log M_{\text{star}} + 0.4K_{200})$, similar to that in Lang et al. (2019). The best-fit linear relation is $M_{\text{star}}/L = 0.55 \times (J_{115} - K_{200}) + 18.92$.

APPENDIX B: TENTATIVE FOREGROUND CONTAMINATION

In this section, we discuss the possibility of contamination caused by a foreground cluster dwarf galaxy. In Figure 1, there is a white core near the center of A2744-DSG-z3. Thus, we demonstrate the grism data to investigate whether it is a foreground contamination. Figure 6 shows the grism data of this contamination candidate. Based on the SED-fitting results, the redshift of this target could be $z = 0.544^{+0.006}_{-0.003}$ given by GRIZLI. We conclude here, only from the grism data, we cannot strongly determine the redshift of this target.

REFERENCES

- Aravena, M., Boogaard, L., González-López, J., et al. 2020, ApJ, 901, 79, doi: [10.3847/1538-4357/ab99a2](https://doi.org/10.3847/1538-4357/ab99a2)
- Astropy Collaboration, Robitaille, T. P., Tollerud, E. J., et al. 2013, A&A, 558, A33, doi: [10.1051/0004-6361/201322068](https://doi.org/10.1051/0004-6361/201322068)
- Astropy Collaboration, Price-Whelan, A. M., Sipőcz, B. M., et al. 2018, AJ, 156, 123, doi: [10.3847/1538-3881/aabc4f](https://doi.org/10.3847/1538-3881/aabc4f)
- Bell, E. F., & de Jong, R. S. 2001, ApJ, 550, 212, doi: [10.1086/319728](https://doi.org/10.1086/319728)

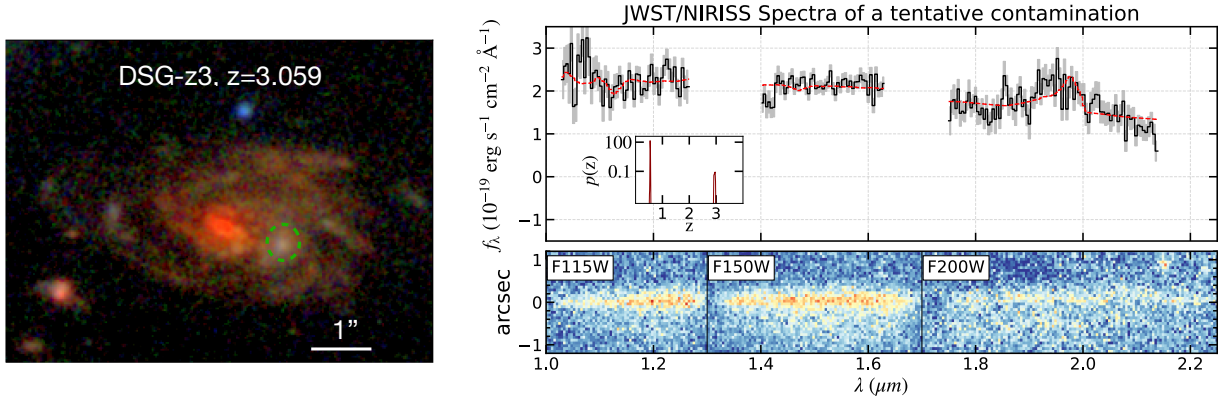


Figure 6. **Left:** Zoom in RGB map (same as Figure 1). The green cycle indicates location of the tentative contamination. **Right:** 2D/1D JWST/NIRISS spectra of the tentative target. Each panel is the same as that in the right panel of Figure 2. We conclude that, from the grism spectra, we cannot directly determine the redshift of the tentative contamination because there are no obvious emission lines. The best-fit redshift of this target could be $z = 0.544^{+0.006}_{-0.003}$. However, there is still a high-redshift solution. Thus, we cannot rule out the possibility that this target is located at the same redshift of A2744-DSG-z3.

- Bolatto, A. D., Wong, T., Utomo, D., et al. 2017, *ApJ*, 846, 159, doi: [10.3847/1538-4357/aa86aa](https://doi.org/10.3847/1538-4357/aa86aa)
- Boyett, K., Mascia, S., Pentericci, L., et al. 2022, arXiv e-prints, arXiv:2207.13459. <https://arxiv.org/abs/2207.13459>
- Calzetti, D., Armus, L., Bohlin, R. C., et al. 2000, *ApJ*, 533, 682, doi: [10.1086/308692](https://doi.org/10.1086/308692)
- Carnall, A. C., McLure, R. J., Dunlop, J. S., & Davé, R. 2018, *MNRAS*, 480, 4379, doi: [10.1093/mnras/sty2169](https://doi.org/10.1093/mnras/sty2169)
- Cen. R. 2014, *ApJ*, 781, 38, doi: [10.1088/0004-637X/781/1/38](https://doi.org/10.1088/0004-637X/781/1/38)
- Chen, C.-C., Gao, Z.-K., Hsu, Q.-N., et al. 2022, arXiv e-prints, arXiv:2208.05296. <https://arxiv.org/abs/2208.05296>
- Chen, Y., Steidel, C. C., Erb, D. K., et al. 2021, *MNRAS*, 508, 19, doi: [10.1093/mnras/stab2383](https://doi.org/10.1093/mnras/stab2383)
- Conselice, C. J. 2014, *ARA&A*, 52, 291, doi: [10.1146/annurev-astro-081913-040037](https://doi.org/10.1146/annurev-astro-081913-040037)
- Conselice, C. J., Blackburne, J. A., & Papovich, C. 2005, *ApJ*, 620, 564, doi: [10.1086/426102](https://doi.org/10.1086/426102)
- Davé, R., Finlator, K., Oppenheimer, B. D., et al. 2010, *MNRAS*, 404, 1355, doi: [10.1111/j.1365-2966.2010.16395.x](https://doi.org/10.1111/j.1365-2966.2010.16395.x)
- Davis, B. L., Berrier, J. C., Shields, D. W., et al. 2012, *ApJS*, 199, 33, doi: [10.1088/0067-0049/199/2/33](https://doi.org/10.1088/0067-0049/199/2/33)
- Dawson, S., McCrady, N., Stern, D., et al. 2003, *AJ*, 125, 1236, doi: [10.1086/367792](https://doi.org/10.1086/367792)
- Elmegreen, B. G. 2002, *ApJ*, 577, 206, doi: [10.1086/342177](https://doi.org/10.1086/342177)
- Elmegreen, B. G., Elmegreen, D. M., Fernandez, M. X., & Lemonias, J. J. 2009, *ApJ*, 692, 12, doi: [10.1088/0004-637X/692/1/12](https://doi.org/10.1088/0004-637X/692/1/12)
- Elmegreen, D. M., & Elmegreen, B. G. 2014, *ApJ*, 781, 11, doi: [10.1088/0004-637X/781/1/11](https://doi.org/10.1088/0004-637X/781/1/11)
- Elmegreen, D. M., Elmegreen, B. G., Yau, A., et al. 2011, *ApJ*, 737, 32, doi: [10.1088/0004-637X/737/1/32](https://doi.org/10.1088/0004-637X/737/1/32)
- Fiacconi, D., Feldmann, R., & Mayer, L. 2015, *MNRAS*, 446, 1957, doi: [10.1093/mnras/stu2228](https://doi.org/10.1093/mnras/stu2228)
- Flewelling, H. A., Magnier, E. A., Chambers, K. C., et al. 2020, *ApJS*, 251, 7, doi: [10.3847/1538-4365/abb82d](https://doi.org/10.3847/1538-4365/abb82d)
- Fudamoto, Y., Inoue, A. K., & Sugahara, Y. 2022, arXiv e-prints, arXiv:2208.00132. <https://arxiv.org/abs/2208.00132>
- Gaia Collaboration, Prusti, T., de Bruijne, J. H. J., et al. 2016, *A&A*, 595, A1, doi: [10.1051/0004-6361/201629272](https://doi.org/10.1051/0004-6361/201629272)
- Gaia Collaboration, Vallenari, A., Brown, A. G. A., et al. 2022, arXiv e-prints, arXiv:2208.00211. <https://arxiv.org/abs/2208.00211>
- Genzel, R., Price, S. H., Übler, H., et al. 2020, *ApJ*, 902, 98, doi: [10.3847/1538-4357/abb0ea](https://doi.org/10.3847/1538-4357/abb0ea)
- Gómez-Guijarro, C., Elbaz, D., Xiao, M., et al. 2022, *A&A*, 658, A43, doi: [10.1051/0004-6361/202141615](https://doi.org/10.1051/0004-6361/202141615)
- González-López, J., Bauer, F. E., Romero-Cañizales, C., et al. 2017, *A&A*, 597, A41, doi: [10.1051/0004-6361/201628806](https://doi.org/10.1051/0004-6361/201628806)
- Gullberg, B., Smail, I., Swinbank, A. M., et al. 2019, *MNRAS*, 490, 4956, doi: [10.1093/mnras/stz2835](https://doi.org/10.1093/mnras/stz2835)
- Hammer, F., Flores, H., Puech, M., et al. 2009, *A&A*, 507, 1313, doi: [10.1051/0004-6361/200912115](https://doi.org/10.1051/0004-6361/200912115)
- Hunt, L. K., Draine, B. T., Bianchi, S., et al. 2015, *A&A*, 576, A33, doi: [10.1051/0004-6361/201424734](https://doi.org/10.1051/0004-6361/201424734)
- Kohandel, M., Pallottini, A., Ferrara, A., et al. 2019, *MNRAS*, 487, 3007, doi: [10.1093/mnras/stz1486](https://doi.org/10.1093/mnras/stz1486)
- Krabbe, A. C., Pastoriza, M. G., Winge, C., et al. 2011, *MNRAS*, 416, 38, doi: [10.1111/j.1365-2966.2011.18946.x](https://doi.org/10.1111/j.1365-2966.2011.18946.x)
- Kroupa, P. 2002, *Science*, 295, 82, doi: [10.1126/science.1067524](https://doi.org/10.1126/science.1067524)
- Lang, P., Schinnerer, E., Smail, I., et al. 2019, *ApJ*, 879, 54, doi: [10.3847/1538-4357/ab1f77](https://doi.org/10.3847/1538-4357/ab1f77)
- Laporte, N., Bauer, F. E., Troncoso-Iribarren, P., et al. 2017, *A&A*, 604, A132, doi: [10.1051/0004-6361/201730628](https://doi.org/10.1051/0004-6361/201730628)
- Law, D. R., Shapley, A. E., Steidel, C. C., et al. 2012, *Nature*, 487, 338, doi: [10.1038/nature11256](https://doi.org/10.1038/nature11256)

- Law, D. R., Steidel, C. C., Erb, D. K., et al. 2009, *ApJ*, 697, 2057, doi: [10.1088/0004-637X/697/2/2057](https://doi.org/10.1088/0004-637X/697/2/2057)
- Li, Z., Wang, X., Cai, Z., et al. 2022, *ApJL*, 929, L8, doi: [10.3847/2041-8213/ac626f](https://doi.org/10.3847/2041-8213/ac626f)
- Lin, C. C., & Shu, F. H. 1964, *ApJ*, 140, 646, doi: [10.1086/147955](https://doi.org/10.1086/147955)
- Madau, P., & Dickinson, M. 2014, *ARA&A*, 52, 415, doi: [10.1146/annurev-astro-081811-125615](https://doi.org/10.1146/annurev-astro-081811-125615)
- Margalef-Bentabol, B., Conselice, C. J., Haeussler, B., et al. 2022, *MNRAS*, 511, 1502, doi: [10.1093/mnras/stac080](https://doi.org/10.1093/mnras/stac080)
- McMullin, J. P., Waters, B., Schiebel, D., Young, W., & Golap, K. 2007, in *Astronomical Society of the Pacific Conference Series*, Vol. 376, *Astronomical Data Analysis Software and Systems XVI*, ed. R. A. Shaw, F. Hill, & D. J. Bell, 127
- Moore, T. J. T., Urquhart, J. S., Morgan, L. K., & Thompson, M. A. 2012, *MNRAS*, 426, 701, doi: [10.1111/j.1365-2966.2012.21740.x](https://doi.org/10.1111/j.1365-2966.2012.21740.x)
- Nelson, E. J., van Dokkum, P. G., Förster Schreiber, N. M., et al. 2016, *ApJ*, 828, 27, doi: [10.3847/0004-637X/828/1/27](https://doi.org/10.3847/0004-637X/828/1/27)
- Oguri, M. 2010, *glafic: Software Package for Analyzing Gravitational Lensing*, *Astrophysics Source Code Library*, record ascl:1010.012. <http://ascl.net/1010.012>
- Rigby, J., Perrin, M., McElwain, M., et al. 2022, arXiv e-prints, arXiv:2207.05632. <https://arxiv.org/abs/2207.05632>
- Rodríguez-Puebla, A., Primack, J. R., Avila-Reese, V., & Faber, S. M. 2017, *MNRAS*, 470, 651, doi: [10.1093/mnras/stx1172](https://doi.org/10.1093/mnras/stx1172)
- Sanders, D. B., Soifer, B. T., Elias, J. H., et al. 1988, *ApJ*, 325, 74, doi: [10.1086/165983](https://doi.org/10.1086/165983)
- Schlawin, E., Leisenring, J., Misselt, K., et al. 2020, *AJ*, 160, 231, doi: [10.3847/1538-3881/abb811](https://doi.org/10.3847/1538-3881/abb811)
- Somerville, R. S., Behroozi, P., Pandya, V., et al. 2018, *MNRAS*, 473, 2714, doi: [10.1093/mnras/stx2040](https://doi.org/10.1093/mnras/stx2040)
- Speagle, J. S., Steinhardt, C. L., Capak, P. L., & Silverman, J. D. 2014, *ApJS*, 214, 15, doi: [10.1088/0067-0049/214/2/15](https://doi.org/10.1088/0067-0049/214/2/15)
- Sun, F., Egami, E., Rawle, T. D., et al. 2021, *ApJ*, 908, 192, doi: [10.3847/1538-4357/abd6e4](https://doi.org/10.3847/1538-4357/abd6e4)
- Sun, F., Egami, E., Fujimoto, S., et al. 2022, *ApJ*, 932, 77, doi: [10.3847/1538-4357/ac6e3f](https://doi.org/10.3847/1538-4357/ac6e3f)
- Tadaki, K.-i., Belli, S., Burkert, A., et al. 2020, *ApJ*, 901, 74, doi: [10.3847/1538-4357/abaf4a](https://doi.org/10.3847/1538-4357/abaf4a)
- Toft, S., Smolčić, V., Magnelli, B., et al. 2014, *ApJ*, 782, 68, doi: [10.1088/0004-637X/782/2/68](https://doi.org/10.1088/0004-637X/782/2/68)
- Treu, T., Roberts-Borsani, G., Bradac, M., et al. 2022, arXiv e-prints, arXiv:2206.07978. <https://arxiv.org/abs/2206.07978>
- Tsukui, T., & Iguchi, S. 2021, *Science*, 372, 1201, doi: [10.1126/science.abe9680](https://doi.org/10.1126/science.abe9680)
- Wang, X., Jones, T., Vulcani, B., et al. 2022, arXiv e-prints, arXiv:2207.13113. <https://arxiv.org/abs/2207.13113>
- Wuyts, S., Förster Schreiber, N. M., Genzel, R., et al. 2012, *ApJ*, 753, 114, doi: [10.1088/0004-637X/753/2/114](https://doi.org/10.1088/0004-637X/753/2/114)